

Austenite stability and M_2C carbide decomposition in experimental secondary hardening ultra-high strength steels during high temperature austenitizing treatments

Abstract:

The present study deals with the austenite stability and M_2C carbide decomposition in three secondary hardening ultra-high strength (SHUHS) steels with varying levels of Cr and Mo (2Cr-1Mo, 2Cr-3Mo and 5Cr-5Mo) investigated using Vicker's hardness, optical and electron microscopy. These steels were subjected to high temperature austenitizing treatments at 1000, 1050, 1100 and 1150°C. It has been established that increasing both Cr and Mo to 5wt. % as well as increasing the austenitizing temperature in this class of SHUHS steels is stabilizing the austenite such that almost 100% austenite is produced upon oil quenching. Further, higher Cr and Mo is also found to influence the stability of metastable M_2C carbide formed during processing of the steels. While the M_2C carbide in 2Cr-3Mo steel remained untransformed, it was found to transform partially to M_6C during austenitization of 5Cr-5Mo steel. Hardness measurements on these steels revealed that hardness is relatively insensitive to austenitizing temperature in 2Cr-1Mo steel, decreased in 2Cr-3Mo and decreased more drastically in 5Cr-5Mo steel with austenitizing temperature. This dependence has been correlated to the influence of composition on M_s temperature and hence on retention of austenite as well as primary carbides. The experimental results were compared against theoretical calculations using ThermoCalc, which predict the presence of only M_6C in both 2Cr-3Mo and 5Cr-5Mo steels. The apparent discrepancy between theoretical and experimental observations has been correlated to kinetic factors.

Keywords: SHUHS steel; EBSD; TEM; M_2C carbide; ThermoCalc

1 Introduction

Cobalt-nickel containing secondary hardening ultra-high strength (SHUHS) steels (e.g. HY180, AF1410, AerMet100 etc.) play an important role as structural materials for niche applications such as aircraft landing gear, armour etc., due to their outstanding combination of high strength, good fracture toughness, K_{IC} and stress corrosion cracking resistance, K_{ISCC} . These are highly alloyed steels containing (in wt. %) 8-16Co, 10-12Ni, 2-3Cr, 1-1.85Mo and 0.1-0.33C [1–3]. Austenitization temperature plays an important role in these steels since it influences several microstructural features e.g.; prior austenite grain size, morphology of martensitic lath structure, volume fraction of primary carbides (carbides retained after austenitizing treatment are called *primary carbides* whereas carbides formed during tempering are called *secondary carbides*), amount of alloying elements dissolved in the austenite and the amount of retained austenite [4–8]. Higher the austenitizing temperature, a greater amount of alloying elements is expected to be dissolved in the austenite [9]; therefore full potential of these alloying elements can be exploited during subsequent quenching-tempering process in which secondary hardening precipitates form. However higher austenitizing temperatures also results in increasing the prior austenite grain size [7,10–14]. At the same time, lower the austenitization temperature, finer is the prior austenite grain size, and greater is the fraction of undissolved primary carbides in the austenite which decreases the secondary hardening effect and also reduces the fracture toughness of the steel [4,15,16]. Prior austenite grain size has direct and indirect effects on mechanical properties of the quenched and tempered steel. While a finer prior austenite grain size results in higher toughness [17,18], it also results in a decrease in the M_s temperature which in turn increases the likelihood of retention of austenite. Retention of austenite in the quenched sample is deleterious to mechanical properties, especially when it transforms to martensite at a later stage during service. Not only does this unstable retained austenite lower the fracture toughness [19], it also indirectly limits the extent of strengthening

achievable during tempering by acting as a sink for carbon. Therefore, it is important to optimize the austenitizing temperature for any new steel composition.

Co-Ni containing SHUHS steel containing 2Cr-1Mo was studied extensively. The nano-scale microstructure of this steel reveals the presence of atomic scale clusters containing Cr, Mo and C [20,21]. It has been established that these clusters have the potential to increase the strength without sacrificing fracture toughness. A study has been undertaken to enhance the strength levels without losing fracture toughness of 2Cr-1Mo steel through minor changes to alloy composition. In order to find the limits on Cr and Mo contents, thermodynamic calculations using ThermoCalcTM [22] have been used extensively. Based on the ThermoCalc results on 2Cr-1Mo steel and the chronological development of typical SHUHS steels (HY180 to AerMet340), a design philosophy has been established to maximize the M₂C fraction and minimize the Cr/Mo ratio of the carbide so as to increase its resistance to coarsening during tempering [23]. The target M₂C fraction in the model alloys was arbitrarily set to be at least 50% higher than that of 2Cr-1Mo steel. Similarly, the Cr/Mo ratio of the carbide was set to at least 50% lower than that in 2Cr-1Mo steel. Using these limits, a combined map of M₂C fraction and Cr/Mo ratio of the carbide in Cr-Mo composition space, at fixed Co, Ni and C contents (in wt. %) of approximately 15, 14 and 0.37 respectively, was generated at typical tempering temperatures. This map has been used as a guide for the selection of alloys, viz., C₂₁, C₂₃ and C₅₅ with (in wt. %) 2Cr-1Mo, 2Cr-3Mo and 5Cr-5Mo respectively. C₂₁ was studied since it is the base composition for comparison to model alloys (C₂₃ and C₅₅). Alloy C₅₅ has 5wt. % each of Cr and Mo and these levels represent the upper bound of Cr and Mo contents. 3wt. % Mo (in alloy C₂₃) is the least amount of Mo required to achieve the design objectives for the same Cr level as C₂₁ and is a conservative alloy composition which still meets the design targets. ThermoCalc results further revealed that the maximum dissolution temperature (T_d) of the precipitates is 1000°C and 1090°C respectively for C₂₃ and C₅₅. However, the respective A₃

temperatures are 729°C and 714°C that are significantly lower than T_d and necessitates the need for a separate study of austenitizing treatments for these novel alloys.

The choice of the range of austenitizing temperatures depends on the class of steels studied and its composition. Typically, higher austenitizing temperatures of 1175°C and up to 1300°C are used for bearing steels and tool steels respectively [10,11,24–26]. SHUHS steels are typically austenitized in the range 800-970°C [3,27,28]. Barring the studies of Schmidt and Gore [29] on solution treatment effects in AF1410 steel, systematic studies of effect of austenitizing temperature on the microstructure and mechanical properties in high Co-Ni containing SHUHS steels are scanty. Further, Schmidt and Gore [29] have essentially focused on the effect of relatively low austenitizing temperatures (816-885°C) on the mechanical properties. The *primary objective* of the present work is to probe the effect of high temperature austenitization temperatures (1000-1150°C) on the stability of different matrix phases in the model alloys (C₂₃ and C₅₅).

It has been reported that the eutectic M₂C carbide formed during solidification in high speed steels transforms to M₆C and MC upon heating above 1000°C [16,30,31]. Hwang et al. [32], have suggested a partial decomposition of M₂C to M₆C when HSS rolls are austenitized at 1100°C for 1h. More recently Li et al. [33] have observed the M₂C decomposition to MC, M₆C and M₇C₃ in tool steels. Presence of M₂₃C₆, M₆C and MC has been reported in SHUHS steels in the as-quenched (AQ) condition [29,34]. However, M₂C carbide was not reported in the AQ condition, although it forms during tempering of SHUHS steels [28,34]. The *second objective* of the present work is to verify whether any carbide decomposition occurs in SHUHS steels which gives rise to formation of M₆C, M₂₃C₆ etc., as reported for AF1410 and AerMet100 steels, upon austenitizing at higher temperatures.

The current work deals with systematic investigation on the influence of austenitizing temperature—1000, 1050, 1100 and 1150°C (for 30 min) and quenching treatments viz. oil-quench (OQ) and oil-quench followed by liquid nitrogen quench (OQ-LN₂) – on hardness and microstructure of quenched samples of C₂₃ and C₅₅ steels. Microstructural characterization has been carried out using optical microscopy, Scanning Electron Microscopy (SEM), Electron Back Scattered Diffraction (EBSD) and Transmission Electron Microscopy (TEM). While most results focus on the newly designed compositions of C₅₅ and C₂₃, these are compared against C₂₁ steel which in composition is similar to the well-studied DMRL SHUHS steel [21,35]. These results are correlated with the thermodynamic calculations using ThermoCalc™.

2 Experimental Procedure

The steels of desired composition were melted and cast in vacuum arc melting furnace from commercially pure raw materials as 450gms pancakes. The pancakes were then soaked at 1100°C for 1h and subsequently hot rolled to 3-4mm thick plates in 2-3 passes by subjecting them to 50-60% reduction. Chemical composition (in wt. %) of the steels, analysed by wet chemical analysis and LECO analyser for C and S contents, is given Table 1. Small samples of size 15x10x4mm were cut from the rolled plates, austenitized in the range from 1000 to 1150°C for 30min at 50°C intervals and then oil quenched to room temperature. ThermoCalc software for Windows OS (TCW5) with TCFE6 database (the database for iron and steel), was used to perform the thermodynamic calculations reported here. Two samples at each austenitizing temperature have been subjected to the austenitization treatment. One sample was preserved after oil quenching and the other was subjected to LN₂ treatment and air warmed to room temperature.

Samples for hardness testing, metallography, SEM and TEM examinations were cut from the heat-treated blanks using slow speed saw. Hardness testing was performed using Vicker's hardness at 30kgf load applied for 10sec. The hardness was measured on at least five different locations on the samples and the mean value along with standard deviation was reported. Samples for optical metallography and SEM were prepared following the standard metallographic techniques and etched with waterless Kalling's reagent. Etched samples were examined using LEICA make optical microscope and Quanta 400D SEM equipped with EDAX.

Table 1 : Chemical compositions (in wt. %) of the experimental steels

Steel	C	Ni	Co	Cr	Mo	Fe
C ₂₁	0.38	14.45	15.68	1.93	0.93	Bal.
C ₂₃	0.36	13.96	15.04	1.95	3.20	Bal.
C ₅₅	0.38	14.05	15.63	5.04	5.10	Bal.

Volume fraction of precipitates (V_f) in samples subjected to different heat treatment conditions was quantified using SEM. For this purpose, the sample surface was divided into at least 24 equal parts and SEM micrographs were captured from each part at 5000X magnification. This method was adopted to obtain better and more uniformly random statistics from the entire area of the sample and to avoid any possible bias while capturing the micrographs. SEM micrographs were analyzed using Image J software [36] and the V_f was calculated as the ratio of number of precipitate pixels to the total number of pixels in the micrograph. Individual V_f 's from all the 24 micrographs for each heat treatment condition were used to calculate the average V_f .

Retained austenite (RA) measurements and precipitate phase mapping were carried out using EBSD technique. Samples for EBSD analysis were initially polished using the standard

metallographic techniques and subsequently on BUEHLER VIBROMET 2 vibratory polisher for 12-15hrs using colloidal silica solution and examined in Zeiss make SUPRA55 FESEM. An area of 100 μ m x 100 μ m was examined using step sizes of 100 and 125nm. Austenite and martensite phase fractions from EBSD images were quantitatively evaluated using AZTec software supplied by Oxford Instruments Inc. Thin foils for TEM examination were prepared by mechanical grinding to ~100 μ m thickness and the central hole was punched by twin-jet electropolishing using mixed acids electrolyte at -30°C. The thin foils were examined in a FEI Tecnai 20T transmission electron microscope operated at 200 kV and equipped with an EDAX EDS system. Chemical composition of the precipitates and matrix was measured, using EDS, on at least 10 different locations in the matrix regions and 10 precipitates and the mean composition along with standard deviation was reported.

3 Results

3.1 Microstructural studies on the majority phases

Samples austenitized at the two extremes of the austenitizing temperature window (i.e. 1000 and 1150°C austenitized samples) were selected for microstructural examination. Although optical microscopy of all the three steels has been conducted, typical micrographs for C₂₃ austenitized at 1000°C and 1150°C in either OQ or OQ+LN₂ condition are shown in Fig. 1. C₂₃ austenitized at 1000°C followed by OQ+LN₂ treatment (Fig. 1a) shows a typical lath martensitic structure. However, upon austenitizing at 1150°C, C₂₃ has an almost fully martensitic structure only in the OQ+LN₂ condition (Fig. 1c). In the OQ condition, two-phase mixture, which is characterized by dark clusters of laths and platelets in a light matrix, is observed (Fig. 1b). C₅₅ also showed the similar lath martensitic structure as C₂₃, when austenitized at 1000°C after OQ+LN₂ treatment. Further, C₅₅ austenitized at 1150°C exhibited

a single-phase austenite and a two-phase microstructure (similar to C_{23} in the OQ condition) in the OQ and OQ+LN₂ conditions respectively. In contrast to C_{23} and C_{55} , C_{21} austenitized at 1000°C and 1150°C in either OQ or OQ+LN₂ condition showed the lath martensitic structure.

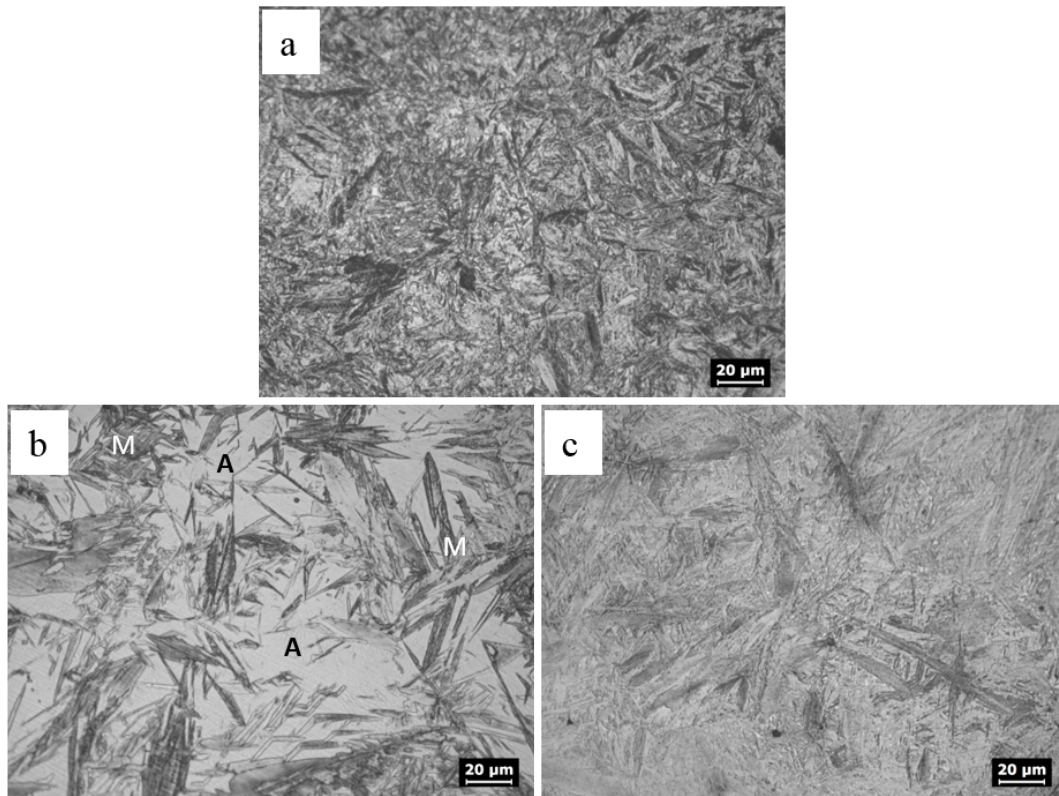


Fig. 1: Optical micrographs of C_{23} austenitized at (a) 1000°C followed by OQ+LN₂, (b) and (c) 1150°C followed by OQ and OQ+LN₂ respectively. A: austenite; M: martensite.

While the lath microstructure is a known signature of martensite, it was unclear what the second phase in the two-phase microstructures was. To identify the second phase and to quantify its relative amount, EBSD studies were conducted on C_{23} and C_{55} samples (ones which exhibit the two-phase microstructure). These studies have confirmed that while the plate-like phase was indeed martensite, the matrix phase was fcc, i.e., austenite. Fig. 2 shows the EBSD phase maps of C_{23} and C_{55} samples austenitized at 1150°C, followed by OQ and OQ+LN₂ treatments. C_{23} in the OQ condition reveals significant fraction of RA (Fig. 2a), which gets substantially reduced after the LN₂ treatment (Fig. 2b). In contrast, C_{55} shows an almost fully austenitic

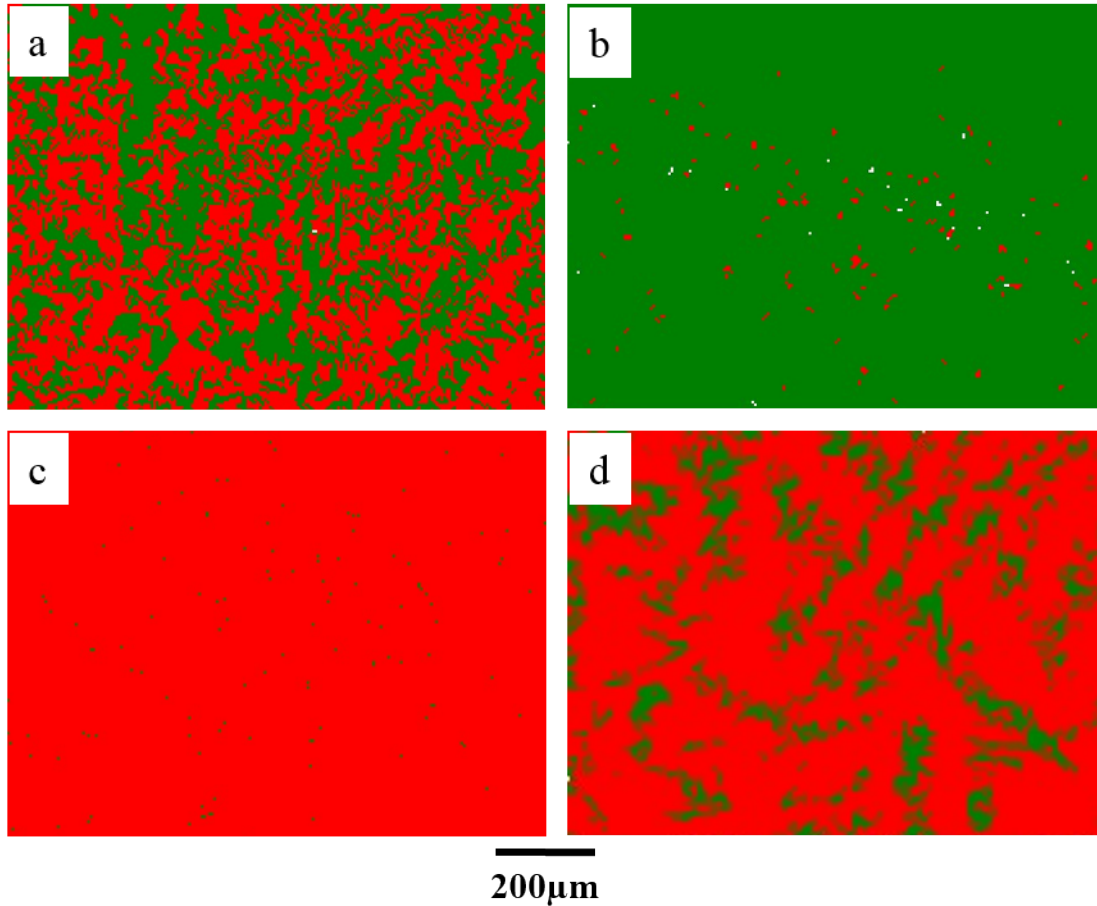


Fig. 2: EBSD phase maps of 1150°C austenitized samples for 30min; (a) C₂₃-OQ, (b) C₂₃-OQ + LN₂, (c) C₅₅-OQ and (d) C₅₅-OQ + LN₂. Red: austenite; Green: martensite.

structure in the OQ condition (Fig. 2c), and a mixture of martensite and RA in the OQ+LN₂ condition (Fig. 2d) with the latter being the dominant phase. The relative proportions of austenite and martensite in C₂₃ and C₅₅, quantified from the EBSD maps, is presented in Table 2. The following features were observed.

- In both steels and for both austenitizing temperatures, OQ followed by LN₂ treatment resulted in lower retention of austenite. For instance, C₂₃ oil-quenched after austenitizing at 1000°C has ~37% RA, whereas C₂₃ which is OQ+LN₂ quenched has only ~2% RA.

- For a given steel and the same quenching treatment, a higher austenitizing temperature results in higher amount of RA. For instance, C₂₃ austenitized at 1000°C and oil-quenched has ~37% RA, whereas C₂₃ austenitized at 1150°C and oil-quenched has 42% RA. These results are consistent with the increase in %RA with austenitizing temperature reported by several researchers [4,37–43].
- Under identical austenitizing and quenching conditions, C₅₅ has higher amount of RA than C₂₃. For instance, OQ after austenitizing at 1000°C results in 37% and 97% RA for C₂₃ and C₅₅ respectively.

Table 2: Relative amounts of retained austenite in C₂₃ and C₅₅ subjected to austenitizing at 1000°C and 1150°C followed by OQ and OQ+LN₂ treatments.

Steel	Austenitizing temperature, ° C	Condition	Area % of austenite	Area % of martensite (= 100-area % of austenite)
C ₂₃	1000	OQ	37.20	62.80
		OQ+LN ₂	2.08	97.92
	1150	OQ	42.10	57.90
		OQ+LN ₂	8.69	91.31
C ₅₅	1000	OQ	96.70	3.30
		OQ+LN ₂	40.70	59.30
	1150	OQ	98.90	1.10
		OQ+LN ₂	56.30	43.70

3.2 Microstructural studies on the minority phases, i.e., primary carbides

In addition to the matrix phases (martensite and austenite), the microstructure of the experimental steels is expected to contain primary carbides (i.e., the minority phases). A detailed SEM, EBSD and TEM study was undertaken to identify and quantify the amount of primary carbides. SEM micrographs of C₂₃ and C₅₅ in as-rolled (AR) and austenitized at 1150°C followed by OQ+LN₂ treatment are shown in Fig. 3. It should be noted that, although SEM of C₂₁ was carried out for measurement of volume fraction of the precipitates, these images are not included in Fig. 3 – C₂₁ did not reveal any primary carbides in the AR condition.

In contrast, SEM micrographs of C₂₃ (Fig. 3a) and C₅₅ (Fig. 3c) in the AR condition reveal the presence of precipitates. While the precipitates in C₂₃ are predominantly coarse (~400nm width and several microns length), a bimodal distribution is observed in C₅₅ with both coarse (~300nm-1.2μm width and few microns length) and fine elongated precipitates (~100nm dia and ~0.6-0.7μm length). C₂₃ and C₅₅ samples austenitized at 1150°C (Fig. 3b and d) also have precipitates, but only the coarse ones.

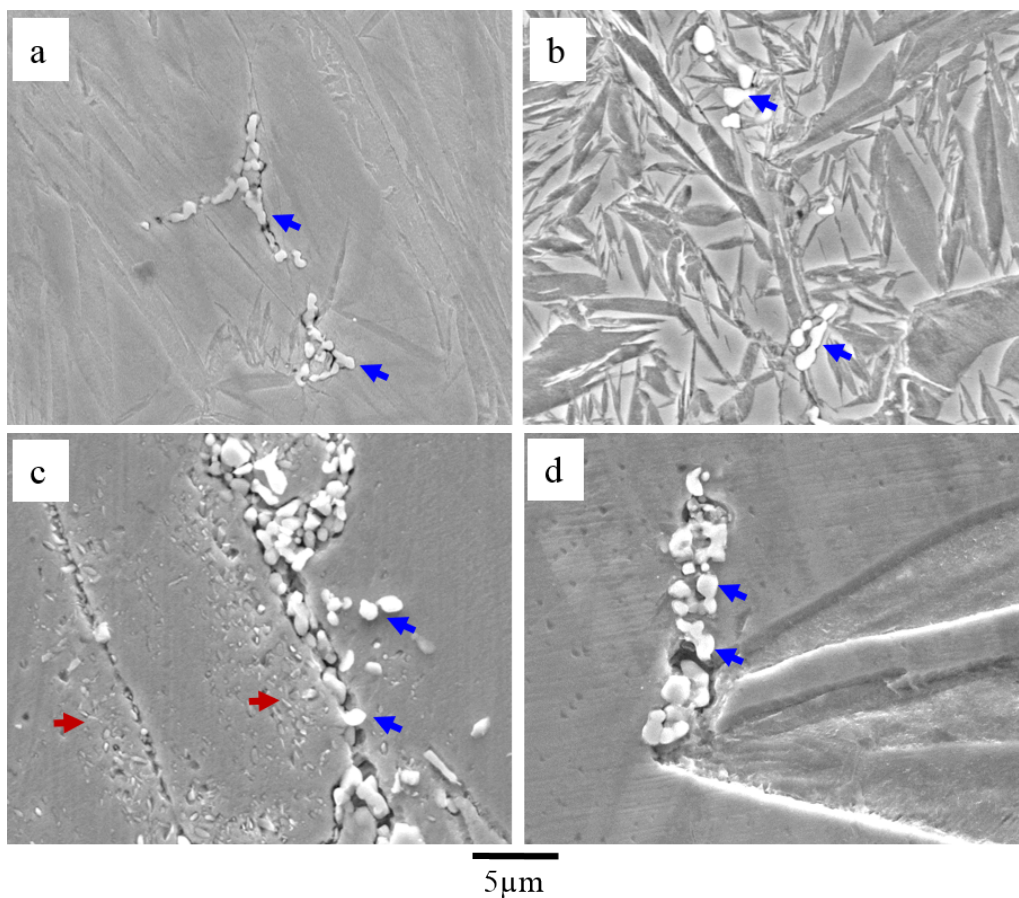


Fig. 3: SEM micrographs showing the presence of precipitates with different sizes and morphologies; (a) C₂₃-as-rolled, (b) C₂₃-austenitized at 1150°C followed by OQ+LN₂, (c) C₅₅-as-rolled and (d) C₅₅-austenitized at 1150°C followed by OQ+LN₂. Coarse and fine precipitates are indicated with blue and red arrows respectively in figure.

To identify the precipitates, diffraction studies were done initially by TEM and subsequently phase mapping was done using EBSD. However, for better readability, EBSD results were

presented first followed by TEM. Fig. 4 shows the EBSD phase maps for C₂₃ and C₅₅ in the AR and 1150°C austenitized samples. Phase maps of C₂₃ (Fig. 4a & b) reveal that only M₂C carbide is present in all heat treatment conditions. In contrast, C₅₅ (Fig. 4c-e) has both M₂C and M₆C, the latter precipitate is observed after austenitization (Figs 4d & e) and not in the AR sample (Fig. 4c). Further, it has been observed that the amount of M₆C was significantly lesser than M₂C.

Both C₂₃ and C₅₅ austenitized at 1000°C followed by OQ+LN₂ treatment (Figs 5 and 6) show the presence of relatively coarse (~1-2µm) and fine (~200nm) precipitates. The fine precipitates have nearly spherical morphology unlike the elongated shape in the AR C₅₅ microstructure (Fig. 3c). EDS analysis of the coarser precipitates (Table 3) reveal that they are enriched with Mo, Fe, and to some extent Cr. These larger precipitates seem to have similar composition in both steels except for the Cr content. The amount of Cr in C₅₅ precipitates is almost double that of C₂₃, which is consistent with the higher amount of Cr in the alloy. Further, EBSD phase maps (Fig. 6) confirm that only M₂C is present in C₂₃ and both M₂C and M₆C are present in C₅₅. These observations are also similar to those found in the AR and 1150°C austenitized samples of C₂₃ and C₅₅ (Fig. 4).

Table 3: Composition (in at. %) of larger precipitates in C₂₃ and C₅₅ austenitized at 1000°C using EDS analysis in SEM.

Steel	Mo	Cr	Fe	Co	Ni
C ₂₃	54.34 ± 4.61	7.93 ± 1.08	27.50 ± 3.88	6.84 ± 0.80	4.38 ± 0.88
C ₅₅	52.35 ± 6.42	14.71 ± 1.06	23.04 ± 4.03	6.42 ± 1.34	4.48 ± 0.99

The foregoing observations (Figs 3 through 6) clearly indicate that the fine precipitates are formed during 1000°C austenitizing treatment. The fine precipitates are not observed in either steel when austenitized at 1150°C. The V_f in all three steels (Table 4) suggests that it is

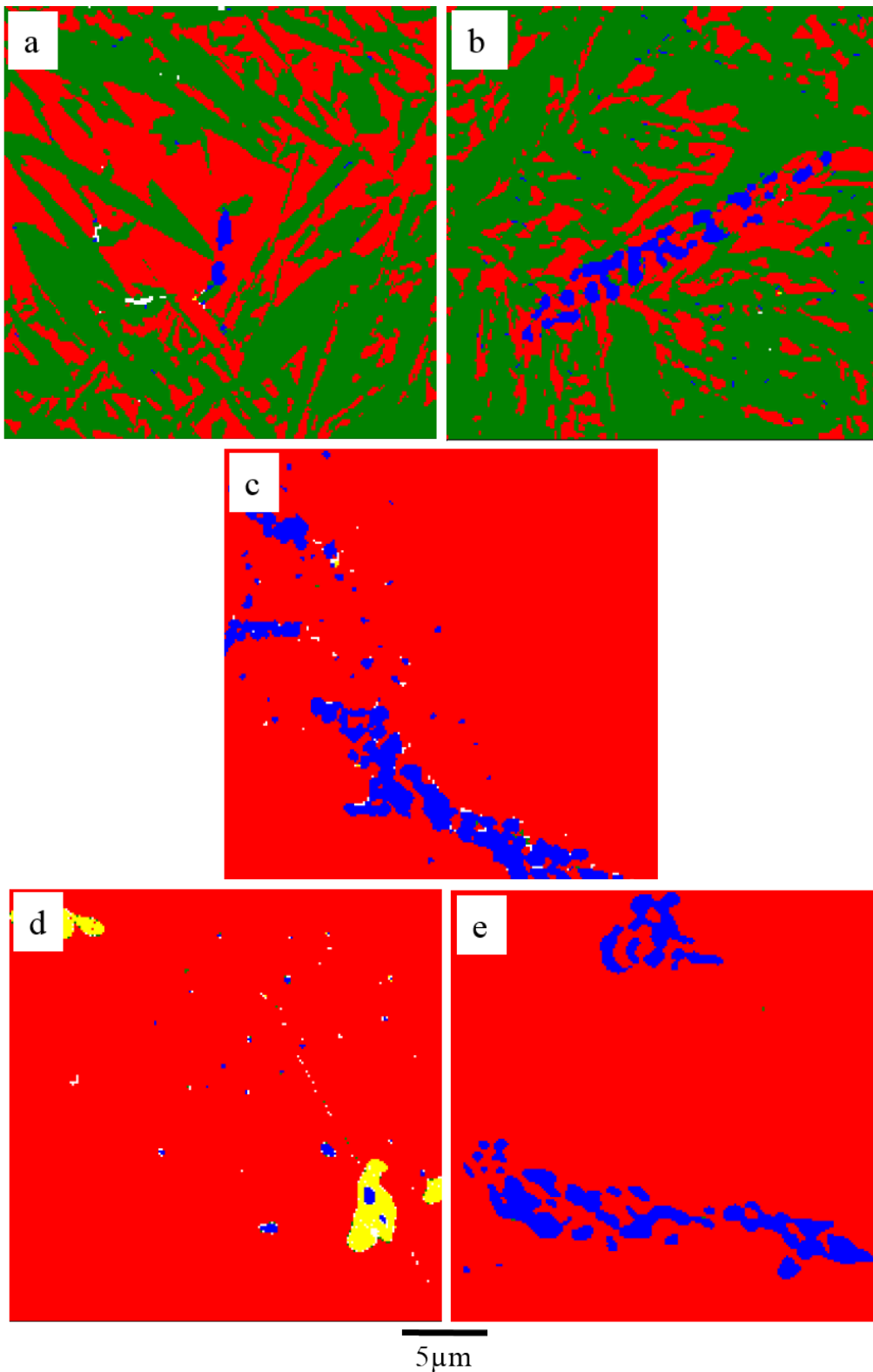


Fig. 4: EBSD phase maps showing the presence of matrix phases and two different types of precipitates; (a) C₂₃-as-rolled, (b) C₂₃-austenitized at 1150°C followed by OQ+LN₂, (c) C₅₅-as-rolled, (d) and (e) C₅₅-austenitized at 1150°C followed by OQ+LN₂. Austenite-red, martensite-green, M₂C carbide-blue and M₆C carbide-yellow.

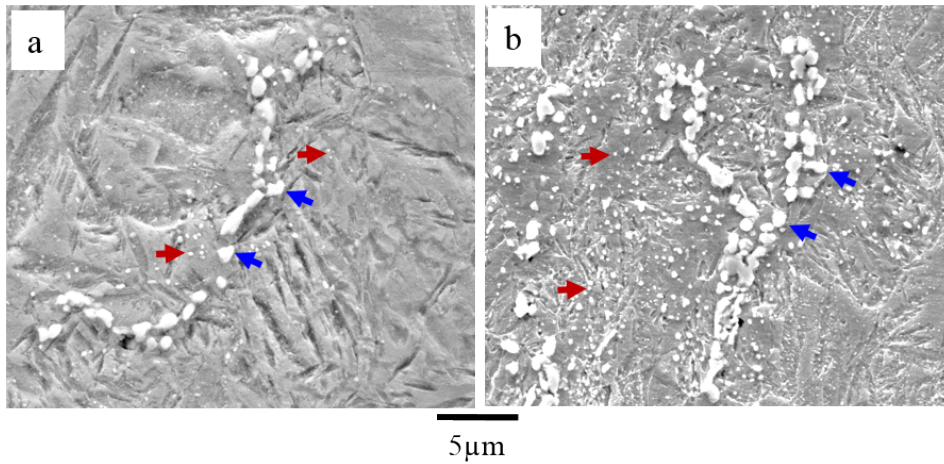


Fig. 5: SEM micrographs of C₂₃ and C₅₅ austenitized at 1000°C followed by OQ+LN₂; (a) C₂₃, and (b) C₅₅. Coarse and fine precipitates are indicated with blue and red arrows respectively in figure.

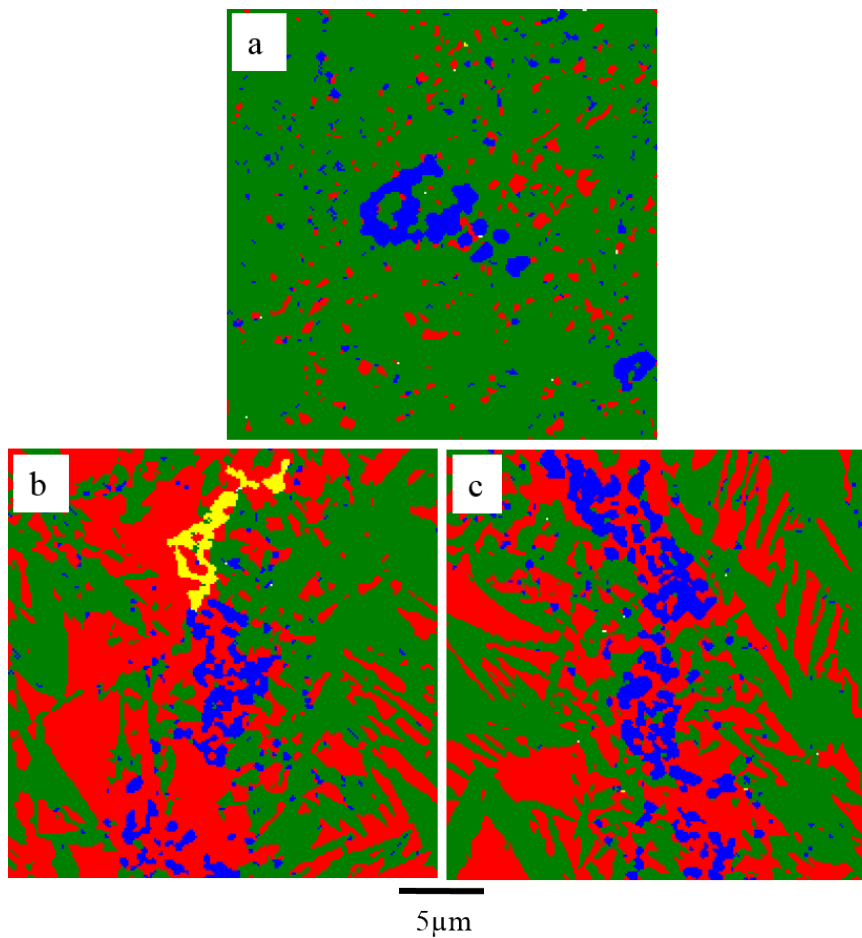


Fig. 6: EBSD phase maps of C₂₃ and C₅₅ austenitized at 1000°C followed by OQ+LN₂ showing the presence of matrix phases and two different types of precipitates; (a) C₂₃, (b) and (c) C₅₅. Austenite-red, martensite-green, M₂C carbide-blue and M₆C carbide-yellow.

significantly higher in the 1000°C austenitized samples compared to the AR samples. However, on austenitizing at 1150°C, the V_f is lower for C₅₅ than that in the AR case and higher for C₂₁ and C₂₃ and significantly lower than samples austenitized at 1000°C.

Table 4: Composition (in at. %) and volume percent of precipitates in different steels austenitized at 1000°C and 1150°C. Carbon was not analyzed/quantified.

Steel	Heat treatment condition	Type of carbide	Volume percent, V_f	Composition (at. %)				
				Mo	Cr	Fe	Co	Ni
C ₂₁	As rolled*	M ₂ C	0.002					
	1000°C*		0.036					
	1150°C*		0.021					
C ₂₃	As rolled*	M ₂ C	0.036					
	1000°C		0.470	88.16±1.63	6.53±0.62	6.24±1.21	-	-
	1150°C*		0.044					
C ₅₅	As rolled*	M ₂ C	0.967					
	1000°C	M ₂ C	1.792	78.26±1.74	14.90±1.29	4.61±0.48	0.99±0.24	1.24±0.17
		M ₆ C		50.42±0.57	7.80±0.28	29.85±0.73	7.75±0.24	4.17±0.31
	1150°C	M ₂ C	0.424	80.94±1.08	12.18±1.33	4.59±0.72	0.90±0.25	1.37±0.22
		M ₆ C		50.43±1.29	6.74±0.41	30.39±1.45	7.82±0.27	4.61±0.09

*Composition of the precipitates was not analysed

To confirm the crystal structure of the primary carbides and to address the possibility of finer carbides that are not resolved by SEM, TEM was conducted. TEM images of C₂₃ austenitized at 1000°C, followed by OQ+LN₂ treatment reveal the presence of precipitates of about 200 nm size (Fig. 7a). Selected area diffraction pattern (SADP) analysis close to $[1\bar{2}1\bar{3}]$ zone axis (Fig. 7b) of these precipitates suggests that these have hexagonal crystal structure with lattice parameters: $a = 3.048\text{Å}$ and $c = 4.58\text{Å}$ and these match well with the theoretical lattice parameters reported for the M₂C carbide [44]. Thus, TEM observations confirmed that these

are indeed hexagonal M_2C -type carbides. Further, composition analysis by TEM-EDS (Table 4) suggests that they are Mo rich with dissolved Cr and Fe. The M_2C particles found in TEM are most likely the finer precipitates observed in SEM micrographs (Fig. 5a). However, the larger particles observed in the SEM or EBSD were not observed in the TEM due to the large spacing between them and small area sampling issues typical of TEM.

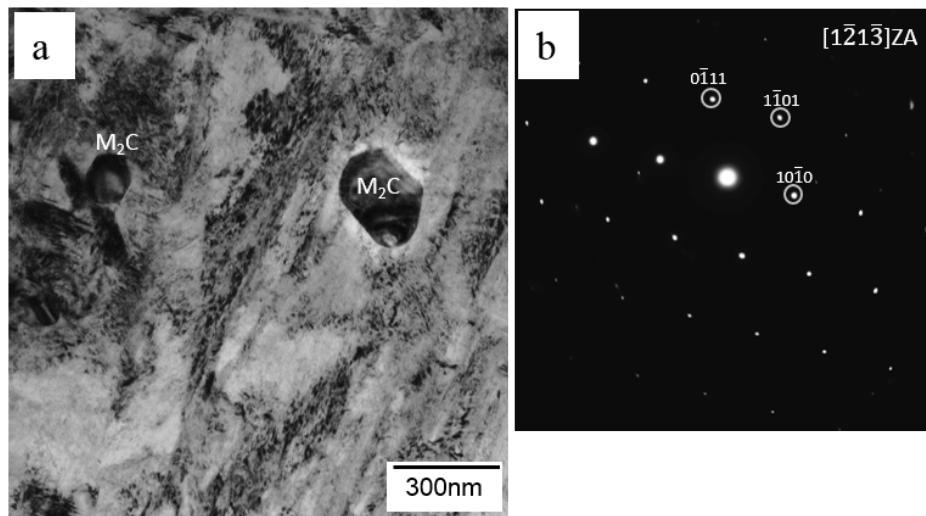


Fig. 7: TEM micrographs of 1000°C austenitized samples in OQ+LN₂ treated condition for C₂₃; (a) BF image and (b) selected area diffraction pattern of the precipitates close to $[1\bar{2}1\bar{3}]$ ZA, confirming that precipitate is hexagonal M_2C type carbide.

Bright field TEM micrograph (Fig. 8a) of C₅₅ austenitized at 1000°C, followed by OQ+LN₂ treatment, reveals the presence of coarse and fine precipitates. SADP analysis of the larger precipitates suggests these can be either M_6C with diamond cubic (DC) or $M_{23}C_6$ with FCC structure. To confirm this, systematic tilting of the sample was conducted from $[001]$ to $[011]$ zone axes (Fig. 8b to c). Although $[111]$ ZA pattern look alike for both DC and FCC structures,

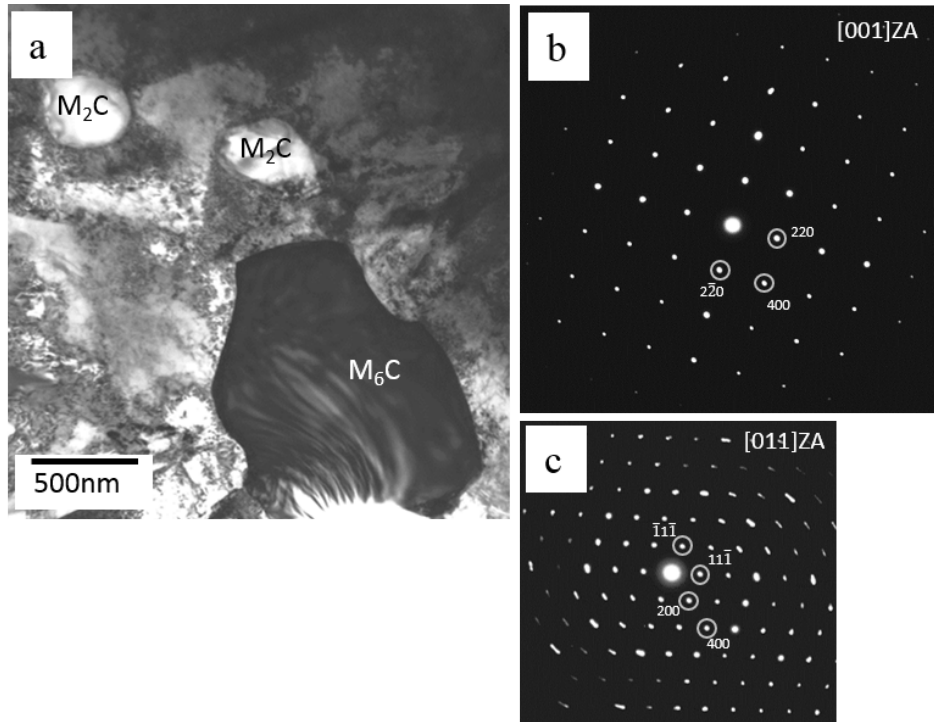


Fig. 8: TEM micrographs of 1000°C austenitized samples in OQ+LN₂ treated condition for C₅₅; (a) BF image and (b) and (c) are selected area diffraction patterns of M₆C precipitate from (a) with [001] and [011] zone axes respectively.

differences can be observed in the [001] and [011] ZA patterns; while (022) spot is a diagonal spot in [011] ZA pattern, it is a side spot in [001] ZA pattern of DC. On the other hand (022) spot remains to be a diagonal spot in both [001] and [011] ZA patterns of the FCC structure. Based on this difference, the larger precipitates were identified as M₆C type carbide with diamond cubic crystal structure containing lattice parameter, $a = 11.05\text{\AA}$, which matches closely with the theoretical value ($a = 11.04\text{\AA}$) reported for the carbide. Diffraction analysis (not shown here) of the finer precipitate confirmed that they are hexagonal M₂C carbides and are similar to M₂C carbides observed in C₂₃. Thus, it is likely that these correspond to the larger and finer precipitates observed in the SEM image (Fig. 5b). TEM-EDS analysis of M₂C and M₆C carbides of C₅₅ in 1000°C and 1150°C austenitizing treatments (Table 4) reveals that at both austenitizing temperatures, M₂C precipitates in C₅₅ has a composition similar to that in C₂₃ except for the higher Cr level, which correlates to higher Cr content in the alloy. M₆C

precipitates are leaner in Mo and richer in Fe, Ni and Co when compared to M_2C precipitates in the same alloy (Table 4). The presence of these other alloying elements in M_6C has been reported previously. Hwang et al.[32] have reported the presence of ~25wt. % Fe in M_6C carbide in high speed steel rolls, while Rong et al. [16] and Moon et al.[45] have observed the presence of Co in M_6C carbide of ASP23, ASP30 and ASP60 high speed steels. However, a comparison of the precipitate composition with the alloy composition suggests that Fe, Ni and Co still partition preferentially to the matrix and not the precipitate. It is interesting to note that while M_6C carbides in C_{55} are Mo rich with Cr/Mo ratio of 1:7, M_6C carbide in AF1410 steel [29] have been reported to be Cr rich with a Cr/Mo ratio of 8:1. It is presently unclear whether these differences arise from differences in alloy composition or not.

Further, it should be noted (Table 4) that the compositions of both carbides is essentially the same after either the 1000°C treatment or the 1150°C treatment. Kim et al., [46] have also observed that the compositions of M_6C , MC and $M_{23}C_6$ carbides in M2 steel were independent of austenitizing temperatures. Therefore, it can be surmised that increasing the austenitizing temperature does not influence the compositions of the precipitates, except for decreasing the volume fraction of the precipitates. Further, changing Cr/Mo levels in the alloy has a scaled effect on Cr/Mo levels in the precipitate.

3.3 Variation of AQ hardness with austenitizing temperature

The variation of AQ hardness as a function of austenitizing temperature for C_{21} , C_{23} and C_{55} is shown in Fig. 9. It is observed that hardness of C_{21} is almost constant with austenitizing temperature (Fig. 9a). There is a minor difference in hardness between OQ and OQ+LN₂ treated samples with the latter samples exhibiting a higher hardness. The hardness of C_{23} in the OQ condition (Fig. 9b) is decreased by ~100VHN when the austenitization temperature was increased from 1000°C to 1050°C; increase in austenitization temperature beyond 1050°C did not decrease the hardness any further. A similar trend in hardness is observed as a function of

austenitizing temperature for C₂₃ in the LN₂ treated condition, although the hardness drop from 1000°C to 1050°C is relatively low (~50VHN). However, the difference in hardness between the OQ and OQ+LN₂ conditions is significantly higher (>100VHN) in this steel when compared to C₂₁. In C₅₅ (Fig. 9c) the hardness gradually decreases monotonically with austenitizing temperature in OQ condition and drastically in the LN₂ treated condition. For almost all austenitizing conditions, C₂₁ shows the highest hardness compared to either C₂₃ or C₅₅ despite higher Cr and Mo in the latter steels. The microstructural origin of these differences in hardness, is discussed in the following sections.

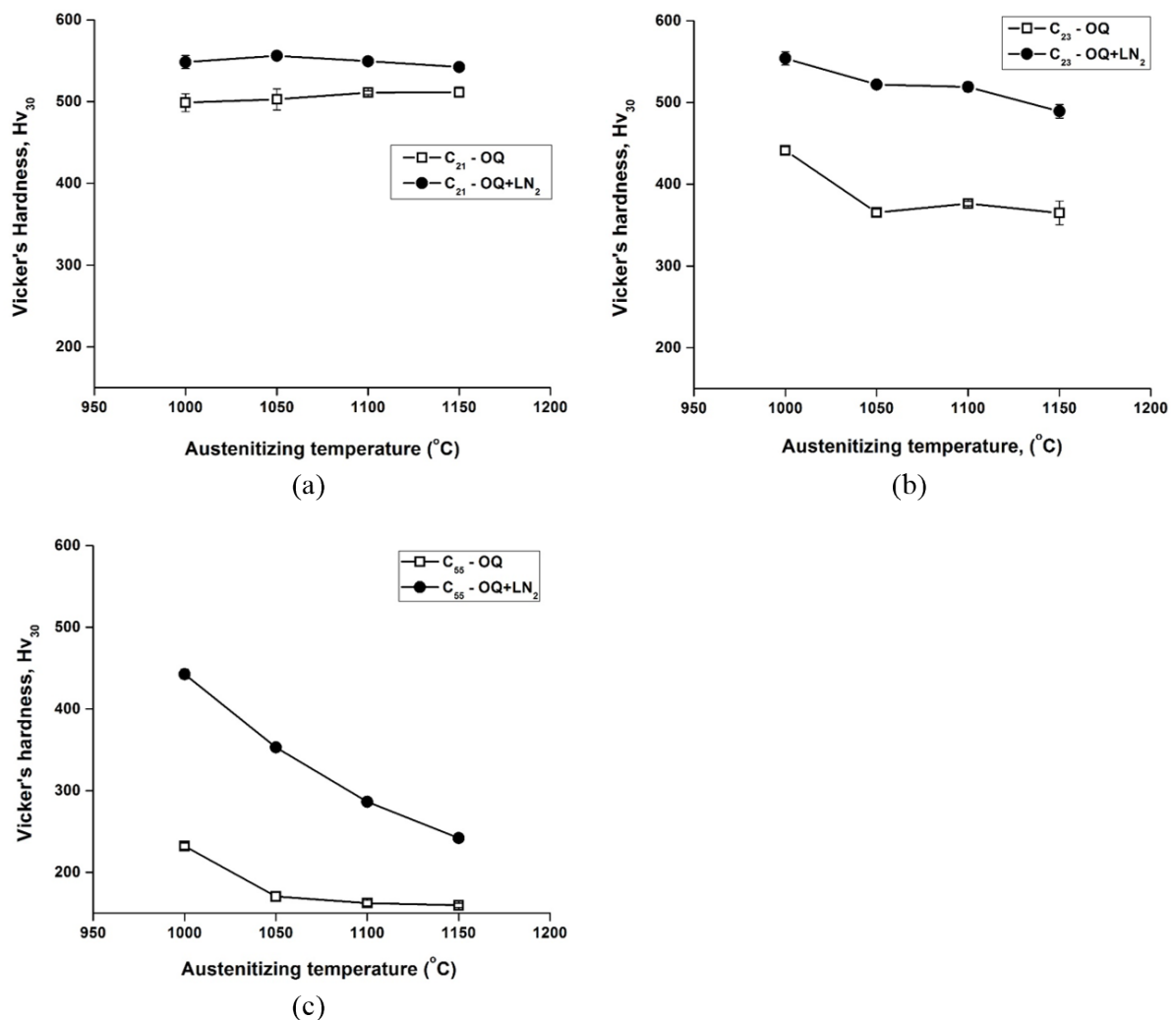


Fig. 9: Effect of austenitizing temperature on hardness of steels: (a) C₂₁, (b) C₂₃ and (c) C₅₅

4 Discussion

4.1 Effect of hardening temperature and LN₂ treatment on matrix phases

It is well known that retention of austenite is the result of the quenching temperature (T_q) lying between the M_s (martensite start) and M_f (martensite finish) temperatures. It has been shown that for both plain carbon steels and tool steels, the fraction of RA can be empirically correlated to the M_s and T_q temperatures via [47,48]:

$$M_s (\text{°C}) = -90.91 * \ln\left(\frac{RA}{100}\right) + T_q \text{ or } RA (\%) = \exp\left(-\frac{M_s - T_q}{90.91}\right) \dots\dots\dots \text{Equation (1)}$$

Typically, M_f is found to be 100-250°C below the M_s temperature depending on the class of steel [49–51]. %RA is strongly dependent on the type of steel, austenitizing temperature and the quenching treatment (i.e., T_q). Our observations suggest that the M_s temperature is sensitive to the alloy composition and the austenitizing treatment. While the former effect is well-known [52], the reason why the austenitizing treatment should affect M_s is presently unclear. Our observation of an increasing %RA with austenitizing temperature suggests that *a higher austenitizing temperature results in a lower M_s* , for the same T_q (refer to Equation 1). A possibility is that higher austenitizing temperature could result in larger grain size which could in turn affect the M_s [43,53–56]. However, larger grain size typically results in higher M_s , since it makes the heterogeneous nucleation of ferrite from austenite grain boundaries more difficult, thus promoting the martensite transformation and thus reduce % RA. So the role of grain size increment can be ruled out.

Indeed, Webster [41] has reported that M_s temperature decreases with increase in austenitizing temperature and this is consistent with our observations. This was attributed to the increased solute concentration in the matrix at high austenitizing temperature due to dissolution of primary carbides. As noted in section 3.2, primary carbides do exist in C₂₃ and C₅₅ steels in the

AR condition. So, it is plausible that their presence affects the matrix (prior-austenite) composition which in turn affects the M_s temperature. The influence of primary carbides on matrix composition and hence on M_s temperature is discussed in the following sections.

4.2 Effect of hardening temperature on precipitate phases

Highly alloyed steels, including SHUHS steels, have been previously shown to contain significant amounts of primary carbides retained from austenitizing treatments. For example, SHUHS steels such as AF1410 [29] were found to contain Cr rich M_6C , Mo rich MC , and also some M_3C carbides in the AQ condition, while AerMet100 steel contained $M_{23}C_6$ and MC carbides [34]. In the AR condition, both C_{23} and C_{55} contain only primary M_2C carbides. Zhou et al. [26] have reported M_2C eutectic carbides with two kinds of morphology in AISI M2 high speed steel depending on the cooling rate; rod like M_2C and lamellar M_2C when the steel was cooled in metal moulds (higher cooling rate) and sand moulds (lower cooling rate) respectively. Since the melting and casting of steels in this present study was performed in a water cooled copper mould, the cooling rates are higher and hence the formation of rod like primary eutectic M_2C carbides is expected. This is indeed consistent with the (rod-like) morphology of M_2C carbides (Figs 3a & c) observed in this study in both C_{23} and C_{55} , although it appears that the carbides have also fragmented during subsequent rolling.

Interesting changes take place in the microstructure when the alloys are subjected to an austenitizing treatment. As seen from Fig. 5 and Table 4, there is a significant increase in the amount of carbides after an austenitization treatment at 1000°C in all three steels. This implies that after this treatment, fresh precipitation of carbides takes place. The aim of typical austenitization treatments is to not only take the steel to the austenite regime, but also to dissolve any pre-existing primary carbides to the maximum extent possible. Clearly, the second objective has not been achieved in the case of 1000°C austenitizing of C_{23} and C_{55} . The 1000°C austenitization treatment acts like an “aging” treatment for all three steels with the fresh

precipitation of secondary carbides. These results are similar to those reported during solution treatment of highly alloyed CrMnN austenitic stainless steels between 750-950°C [57].

Furthermore, fine spherical carbides were observed in both steels after the 1000°C treatment. It is interesting to note that there is a difference between the composition of coarse (from SEM, Table 3) and fine precipitates (via TEM, Table 4). TEM results suggest that the finer precipitates are more highly enriched in Mo compared to the coarse precipitates detected by SEM, despite both precipitates being of M_2C type. This could be due to the enhanced interaction volume in an SEM due to which matrix elements (particularly Fe) would contribute to precipitate's characteristic X-rays. However, it is more likely that these compositional differences are real and not artifacts of the measurement method given the significant difference in composition. It can be surmised that the coarse ones characterized with the SEM precipitated during rolling and prior treatments, while fine ones characterized by TEM formed during austenitization. Since different precipitates emerged from the matrix at different stages and temperatures, they are likely to have the equilibrium composition consistent with the temperature at which they were formed and the prevalent local matrix composition (for e.g., the matrix is leaner in Cr and Mo when the fine precipitates form since some amount of these elements gets locked up in the primary precipitates which formed during rolling and prior treatments). Moreover, it is noted that the M_2C carbide that forms during austenitization has a very low Cr/Mo ratio (i.e. Mo rich, compare Tables 3 and 4). Indeed, ThermoCalc also predicts that M_2C which forms at relatively high temperatures (i.e. above $A_3 \approx 729^\circ\text{C}$) contains extremely low Cr/Mo ratios (0.75 and 0.21 at 600°C and 800°C respectively).

When the steels were austenitized at 1150°C, the V_f decreased significantly (Figs 3b & d and Table 4). The decrease in V_f from 1000°C to 1150°C was found to be 90% and 75% in C_{23} and C_{55} respectively. Compared to the AR condition, there is an increase in the fraction of precipitates due to 1150°C austenitizing treatment for C_{21} and C_{23} , while this fraction is lower

for C₅₅. This suggests that precipitation of carbides continues even at 1150°C in C₂₁ and C₂₃, while it is starting to dissolve in C₅₅. This also hints at the stability of M₂C carbides even at 1150°C especially in C₂₃.

The V_f in C₅₅ is significantly higher than in C₂₃ under all conditions; e.g., in the AR condition C₅₅ contains nearly 1% precipitates against 0.04% in C₂₃. Indeed, significant amounts of undissolved carbides remain even after 1150°C austenitizing treatment in the highly alloyed C₅₅ while the amounts in C₂₃ are negligible. In the present case, the higher amounts of carbides in C₅₅ can be attributed to the relatively higher amounts of Cr and Mo in C₅₅. Lee et al.,[39] report that the residual carbides persist even up to solidus temperature in tool steels. Thus, while 1150°C austenitizing treatment may suffice for C₂₃, C₅₅ requires temperatures much greater than 1150°C for complete dissolution of carbides. These results are also consistent with the ThermoCalc prediction of higher dissolution temperature (T_d) for C₅₅ (1090°C) compared to C₂₃ (1000°C). Since ThermoCalc under predicts critical temperatures and does not consider the kinetics, the absolute value of T_d is less significant than the change in T_d with composition. Moreover, the type of secondary carbide present after the austenitization treatment is also different. While C₂₃ was found to contain only M₂C in the AR condition and after austenitizing (at both 1000°C and 1150°C), C₅₅ was found to contain M₂C carbide in the AR condition and M₂C as well as M₆C carbides in the austenitized-quenched condition. Schmidt and Gore [29] have previously reported a similar presence of M₆C carbides in AF1410 steel subjected to 830°C austenitizing treatment. Thus, it is proposed that M₂C carbides are relatively less stable than M₆C carbides in C₅₅ whereas it is more stable in C₂₃. It has been suggested that in high speed steels, M₂C formed as eutectic carbide during solidification transforms to M₆C and MC when heated above 1000°C [16,30,31]. It is hypothesized that a similar phenomenon occurs in C₅₅ also; M₂C carbides partially dissolve to reprecipitate as M₆C carbides on austenitizing. The stability and the composition of M₆C carbides is dependent on alloy composition.

4.3 Influence of precipitate dissolution on austenite stability

The increase in austenitization temperature from 1000°C to 1150°C decreased the amount of carbides significantly in both C₂₃ and C₅₅. Since these precipitates are rich in Mo, Cr and C, their formation and dissolution is expected to affect the austenite composition as well. The matrix composition based on TEM-EDS analysis at 1000°C and 1150°C in C₅₅ steel (Table 5) clearly reveals that Mo content of the matrix increases significantly in the 1150°C austenitized sample. Also shown in the table is the alloy composition for reference. Since these measurements were done using TEM-EDS, carbon content could not be measured reliably. However, one can estimate the carbon in austenite by doing a mass balance where the following information is utilized:

- volume fraction of the carbides at the two austenitization temperatures in C₅₅
- the measured composition of carbides, and
- the assumption that the carbide is M₂C and stoichiometric

Table 5: Matrix composition (at. %) in C₅₅ austenitized at 1000°C and 1150°C using EDS analysis in TEM.

Austenitizing temp., °C	Mo	Cr	Co	Ni	Fe	C
1000°C	2.75±0.07	6.28±0.14	15.13±0.07	12.56±0.30	62.07±0.24 ^{\$}	1.19 [#]
1150°C	3.20±0.20	5.69±0.23	15.04±0.18	13.92±0.16	60.48±0.34 ^{\$}	1.65 [#]
Alloy composition	3.02	5.51	15.09	13.62	60.97	1.79

estimated value

\$ value after deducting carbon from the measured Fe in TEM-EDS analysis

The amount of carbon in austenite in Table 5 was estimated by subtracting the carbon locked up in the undissolved precipitates (whose volume fraction was obtained from the SEM, Table 4) from that in the alloy. Table 5 clearly shows that Cr, Mo and C levels in austenite change

significantly with austenitization temperature. The enrichment of Mo, Cr and C in austenite at higher austenitizing temperature is expected to decrease the M_s temperature and thus result in retardation of austenite decomposition.

Several functions have been defined to correlate the M_s temperature to the composition of austenite. Kung and Rayment [52] suggested that Steven and Haynes and Andrew's linear equations predicted M_s accurately to within 25°C in 80-85% of high alloy steels. These formulae are given below:

Steven and Haynes: M_s (°C) = 561-474C-33Mn-17Cr-17Ni-21Mo+(10Co-7.5Si)
Equation (2)

Andrews: M_s (°C) = 539-423C-30.4Mn-12.1Cr-17.7Ni-7.5Mo+ (10Co-7.5Si)...Equation (3)

Using these equations, the M_s temperature was predicted for the matrix composition of C₅₅ austenitized at 1000°C and 1150°C (Table 5). Although the two formulae predict different values for M_s temperature, both predict similar trends, i.e., the M_s temperature for C₅₅ decreases at the higher austenitizing temperature of 1150°C (Fig. 3d & 5b and Table 4). These conclusions are similar to those reported by Webster [41].

It is acknowledged that the method of estimating austenite composition is approximate, but the aim of the exercise was to qualitatively demonstrate the effects of austenitization temperature. Instead of experimental composition of austenite, one could calculate the composition of austenite using ThermoCalc. This exercise was attempted next.

Either equation (2) or (3) can be used for estimating the M_s temperature in high strength steels. However, Stevens and Haynes equation appear to predict the M_s more closely for the experimental steels. Thus, equation (2) was used for estimating the M_s temperature from ThermoCalc based austenite composition and compared against the M_s temperature predicted from the RA measurements through EBSD and shown in Table 6. It can be seen that there are

significant differences between the M_s temperatures calculated from the two empirical equations (1) and (2). However, the predicted trends in variation of M_s temperature with austenite composition and hence the austenitizing temperature from both the equations are comparable and similar to that from experimental composition measurements. Though matrix composition was not estimated experimentally in C_{23} , it is reasonable to conclude that in this case as well, the higher temperature austenitization would have resulted in higher amounts of Cr, Mo and C in austenite (which was confirmed by ThermoCalc) resulting in lower M_s and hence greater amount of RA. It can thus be summarized that the decrease in M_s due to higher dissolution of carbides at higher temperatures results in a greater amount of RA resulting in lower hardness. Table 6 shows that the depression of M_s is more severe in C_{55} .

Table 6: Comparison of calculated M_s temperatures from RA measurements in EBSD and austenite composition from ThermoCalc using the empirical formula found in ref. [47,48,52]

Alloy	Aust. Temp. (°C)	Predicted value of M_s^* (°C)	Estimated value of M_s^{**} (°C)	Estimated value of $M_f^\#$ (°C)	Precipitate fraction [§] (%)
C_{23}	1000	210	120	-130	0.47
	1150	203	109	-141	0.04
C_{55}	1000	185	33	-217	1.79
	1150	104	31	-219	0.42

*based on ThermoCalc composition of austenite and the Stevens and Haynes formula for M_s temperature.

**based on % RA obtained from EBSD measurements in oil quenched condition

assumed to be estimated $M_f = (M_s - 250^\circ\text{C})$

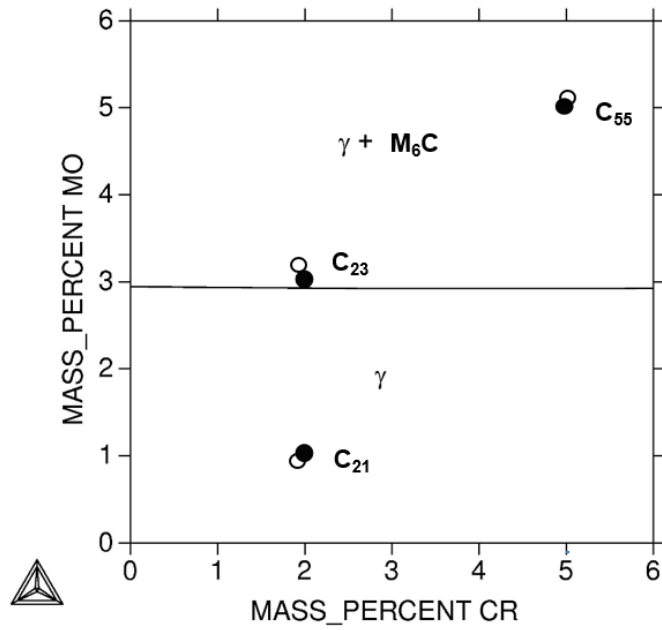
§area fraction measurements in SEM

4.4 Thermodynamic justification for the observations

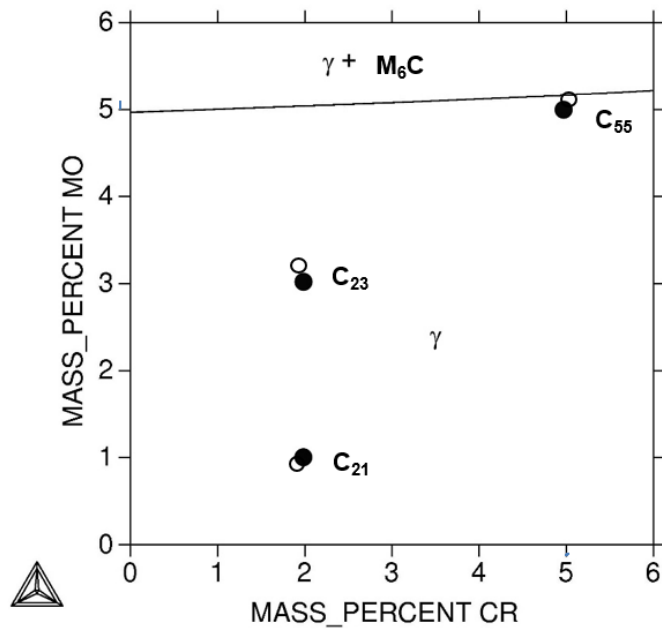
The experimental observation of the different carbides and their evolution in the austenitizing regime, in C_{23} and C_{55} , can be correlated with theoretical calculations using ThermoCalc. Fig. 10 shows isothermal calculations at the experimental austenitizing temperatures (1000°C and

1150°C) reported in this study, at a fixed composition of 0.37C-15Co-14Ni. At 1000°C austenitizing (Fig. 10a), these calculations suggest the presence of austenite and limited amounts of M_6C in C_{23} (i.e., closer to the phase boundary) and austenite with significant amounts of M_6C in C_{55} (i.e., deep in the $\gamma+M_6C$ phase field). Clearly, the prediction of M_6C lends support to its experimental observation. Interestingly, M_2C carbides are not predicted by ThermoCalc for either alloy. However, experimental results using TEM and EBSD reveal the presence of only M_2C in C_{23} (Figs 4a-b, 6a & 7) and predominantly M_2C and small amount of M_6C in C_{55} (Figs 4c-e, 6b-c & 8). It is more likely that a fraction of the observed M_2C carbides in the austenitized condition are those retained from the AR condition. The second probable cause of the discrepancy is that though M_6C is thermodynamically more stable (as confirmed by Grujicic [58]), its formation which is accompanied by the dissolution of M_2C is perhaps sluggish for kinetic reasons. However, since ThermoCalc predicts the formation of equilibrium phases only and does not account for kinetics, M_6C carbide is predicted. Lastly, some of these differences can also be attributed to probable inaccuracies in the thermodynamic database itself.

A similar discrepancy between ThermoCalc predictions and experiments is also seen at 1150°C. At 1150°C austenitizing (Fig. 10b), both steels fall in the single-phase austenite region. However, experimental results show that C_{23} contains a small fraction (0.04 %) of M_2C (Fig. 3b), while C_{55} shows relatively higher amounts (0.4%) of M_2C and M_6C (Fig. 3d). These results are similar to those in Fe-17Cr-0.5C steel austenitized at 1200°C for 15min, where experiments revealed the presence of carbides, while ThermoCalc predicted single phase austenite at this temperature [59]. It is worth noting that at both temperatures (Figs 10a & b), C_{21} always falls in a single-phase austenite regime, which is consistent with experiments. The relative insensitivity of the hardness of AQ C_{21} to austenitization temperature (Fig. 9a) is indicative that the austenite composition does not change with austenitization temperature (as it does for



(a)



(b)

Fig. 10: Isothermal sections at (a) 1000°C and (b) 1150°C as a function of Mo and Cr concentrations at a fixed composition of 0.37C-15Co-14Ni. Compositions of designed and experimental steels of C₂₁, C₂₃ and C₅₅ are indicated with black spheres and open circles respectively on both (a) and (b).

C₂₃ and C₅₅) and this in turn is because at and above 1000°C, C₂₁ is always in single phase regime. On the other hand, in C₂₃ and C₅₅ an increase in austenitization temperature from 1000 to 1150°C reduced the amount of primary carbides. Clearly, the reduction in the amount of carbide at higher austenitization temperature also implies a greater amount of Cr/Mo and C in solution, which results in a lower M_s temperature and lower AQ hardness (Fig. 9b & c).

4.5 Effect of austenitizing temperature on AQ hardness

Several conflicting results exist on the effect of austenitizing temperature on the strength or hardness of quenched steels. One surmise that composition of the steel plays a significant role in influencing the specific effect of austenitizing temperature on strength/hardness. For instance, several authors [39,45,56,60–63] have reported an increase in hardness/strength, while others [14,29,40,53,64] have observed a decrease with austenitizing temperature. Yet other researchers [43,65–68] have also found that the strength/hardness remains relatively unaffected by austenitizing temperature. These studies involved different classes of steels such as secondary hardening steels, low alloy steels, high speed steels and ultra-high strength steels. Occasionally even for the same steel, conflicting behaviors have been reported. For instance, in AISI 4340 steel, Tomita [62] has reported an increase in strength, while Lai et al.,[43] have found that it remains fairly constant with austenitizing temperature.

In the present study, the three steels under investigation were found to exhibit three different dependences of AQ hardness on austenitizing temperatures. C₂₁ shows a hardness that is nearly independent of austenitizing temperature, while C₂₃ and C₅₅ exhibit a decrease in hardness with austenitizing temperature. Decrease in hardness with austenitizing temperature has been attributed previously to phenomena such as auto tempering [29] and grain growth [40,64]. However, in the present work, microstructural evidence strongly points to the fact that the decrease in hardness with austenitizing temperature, in both C₂₃ and C₅₅, is related to the concomitant increase in RA. The amount of RA was observed to increase from 1000°C to

1150°C for both steels (Table 2). Fig. 11 correlates the AQ hardness with the corresponding %RA. This plot combines data for all three alloys subjected to a variety of austenitization treatments and quenching conditions. It is interesting to note that the AQ hardness for the three different alloys subjected to different treatments falls on a master curve when plotted as a function of %RA. Such a convergence across alloys strongly suggests that AQ hardness is largely determined by %RA and not directly by compositional differences. The effects of composition and austenitization temperature on AQ hardness is indirect and via its influence on %RA.

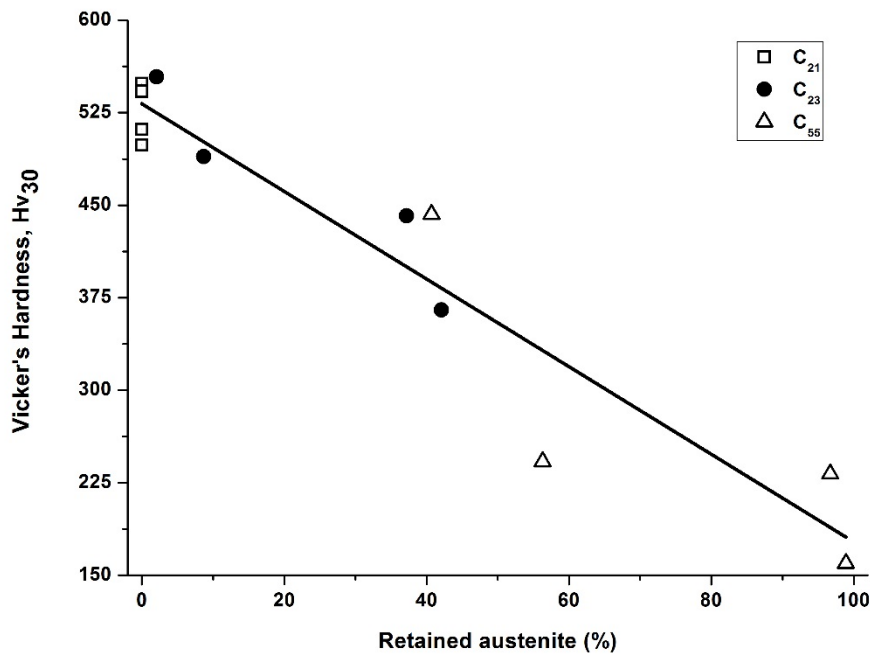


Fig. 11: Variation of hardness as function of retained austenite (%) in three steels austenitized at 1000°C and 1150°C followed by OQ and OQ+LN₂ treatments.

This study clearly reveals that there exists an upper bound to the Cr and Mo levels in SHUHS steels, beyond which the presence of significant amount of RA cannot be avoided even after LN₂ treatment. At high levels of Cr and Mo (C₅₅), partial decomposition of M₂C to M₆C has been observed upon austenitizing. Although, the decomposition of metastable M₂C into MC

and M_6C is commonly observed in tool steels, such decomposition in high Co-Ni containing SHUHS steels is observed for the first time. Further, a considerable fraction of un-dissolved primary carbides remains in the austenite even after austenitizing at 1150°C. Consequently, the precipitation of secondary hardening carbides upon tempering is severely reduced due to the locking up of the constituent elements in the primary undissolved carbides. Under such conditions, when high amounts of RA and undissolved primary carbides exist, the steel ceases to be a martensitic secondary hardening steel.

5 Conclusions

In this work, the austenite stability and M_2C carbide decomposition during high temperature austenitizing treatments was investigated in experimental secondary hardening steels with varying amounts of Cr and Mo. The main conclusions from this work are as follows:

- Increase in Cr and Mo and austenitization temperature has resulted in increasing the stability of the austenite.
- Volume fraction of precipitates was found to be highest in C_{55} followed by C_{23} and C_{21} in all heat treatment conditions.
- 1000°C austenitization treatment acts more like an “aging” treatment instead of a solutioning treatment in C_{23} and C_{55} .
- Metastable M_2C carbide in C_{55} transforms partially to M_6C during austenitizing, while such transformation is not observed in C_{23} .
- C_{21} exhibited a higher hardness in the AQ condition compared to either C_{23} or C_{55} at all austenitizing temperatures. Further, the hardness of C_{21} was found to be relatively insensitive to the austenitizing temperature.

6 Acknowledgements

This research was funded by the Defence Research and Development Organization (DRDO), India. The permission of Dr. Vikas Kumar, Scientist ‘H’, Director, Defence Metallurgical Research Laboratory (DMRL), Hyderabad, to publish the results is gratefully acknowledged. The authors wish to thank Dr. M. Srinivas, Scientist ‘G’ (retired) for fruitful discussions while performing this work. The authors are grateful to Professor T. A. Abinandanan, Chairman, Dept. Materials Engg., IISC, Bangalore, Dr. K. Muraleedharan, Scientist ‘G’, Director, CGCRI, Kolkata, Dr. G. Malakondaiah, former Director, DMRL and former Chief Controller (HR&D) at DRDO Headquarters, Dr. S. V. Kamat, Distinguished Scientist, former Director, DMRL and DG (NS&M) and Dr. P. Ghosal, Group Head, Electron Microscopy Group, DMRL for their constant encouragement and support. The authors also wish to thank Mr. Deepak Kumar for his help in preparing thin foils for TEM investigations and Mr. Vajinder Singh for his help with EBSD measurements.

7 References

- [1] L.E. Iorio, J.L. Malony, W.M. Garrison Jr., 40th Mechanical Working and Steel Processing Conf. Proc., ISS-AIME, in: Warrendale, PA, 1999: pp. 901–920.
- [2] J.M. Dahl, P.M. Novotny, Airframe and landing gear alloy, *Adv. Mater. Process.* 155 (1999) 23–25.
- [3] About Carpenter Technology - specialty alloy development and manufacturing supported by industry-leading materials expertise, (n.d.). <http://www.cartech.com/search.aspx?searchtext=AerMet> (accessed August 16, 2014).
- [4] K. Soto, Improving the Toughness of Ultrahigh Strength Steel, University of California, 2002. <http://www.osti.gov/scitech/biblio/803864> (accessed December 29, 2013).
- [5] I. Souki, D. Delagnes, P. Lours, Influence of heat treatment on the fracture toughness and crack propagation in 5% Cr martensitic steel, *Procedia Eng.* 10 (2011) 631–637. doi:10.1016/j.proeng.2011.04.105.
- [6] G. Hande, E. Rukiye, Ö. Resat, Effect of heat treatment on the microstructure and mechanical properties of 30MnB5 boron steel, *Mater. Technol.* 48 (2014) 971–976.
- [7] L. Yiwa, G. Hanjie, S. Xiaolin, M. Mingtao, G. Jing, Effects of Austenitizing Conditions on the Microstructure of AISI M42 High-Speed Steel, *Metals.* 27 (2017) 1–13. doi:10.3390/met7010027.

- [8] H. Lianfang, L. Huiping, W. Cheng, Effect of Austenitization Temperature on Microstructure and Mechanical Properties of B1500HS Boron Steel in the Hot Stamping, *MATEC Web Conf.* 67 (2016) 1–7. doi:DOI: 10.1051/mateconf/20166703001.
- [9] J. Changhong, T. Di, Z. Aimin, Z. Yan, Z. Cong, Effect of Austenizing Temperature and Time on Microstructure and Mechanical Properties of Cr12MoVNbRE Steel, *Mater. Sci. Forum.* 788 (2014) 372–377. doi:10.4028/www.scientific.net/MSF.788.372.
- [10] L.A. Dobrzański, The structure and properties of W-V high-speed steels with increased content of silicon, *J. Mater. Process. Technol.* 56 (1996) 933–944. doi:10.1016/0924-0136(96)85121-1.
- [11] J. Sjöström, J. Bergström, Thermal fatigue testing of chromium martensitic hot-work tool steel after different austenitizing treatments, *J. Mater. Process. Technol.* 153–154 (2004) 1089–1096. doi:10.1016/j.jmatprotec.2004.04.158.
- [12] S.M.A. Al-Qawabah, S.R. Khalid, A. Ahmad, The Effect of Austenite Temperature on the Microstructure, Mechanical Behavior, Hardness, and Impact Toughness of AISI D2 Tool Steel, *Int. J. Eng. Res. Appl.* 2 (2012) 2890–2896.
- [13] H. Babaei, K. Amini, A. Shafyei, The effect of heat treatment on mechanical properties and microstructure of the AISI 422 martensitic stainless steel, *MECHANIKA.* 22 (2016) 576–580.
- [14] H. Hou, L. Qi, Y.H. Zhao, Effect of austenitizing temperature on the mechanical properties of high-strength maraging steel, *Mater. Sci. Eng. A.* 587 (2013) 209–212. doi:10.1016/j.msea.2013.08.070.
- [15] J. Adamczyk, E. Kalinowska-Ozgowicz, W. Ozgowicz, R. Wusatowski, Interaction of carbonitrides V(C,N) undissolved in austenite on the structure and mechanical properties of microalloyed V-N steels, *J. Mater. Process. Technol.* 53 (1995) 23–32. doi:10.1016/0924-0136(95)01958-H.
- [16] W. Rong, H.-O. Andrén, H. Wisell, G.L. Dunlop, The role of alloy composition in the precipitation behaviour of high speed steels, *Acta Metall. Mater.* 40 (1992) 1727–1738. doi:10.1016/0956-7151(92)90116-V.
- [17] T. Hanamura, F. Yin, K. Nagai, Ductile-Brittle Transition Temperature of Ultrafine Ferrite/Cementite Microstructure in a Low Carbon Steel Controlled by Effective Grain Size, *ISIJ Int.* 44 (2004) 610–617. doi:10.2355/isijinternational.44.610.
- [18] S. Morito, H. Saito, T. Ogawa, T. Furuhashi, T. Maki, Effect of Austenite Grain Size on the Morphology and Crystallography of Lath Martensite in Low Carbon Steels, *ISIJ Int.* 45 (2005) 91–94. doi:10.2355/isijinternational.45.91.
- [19] F.G. Caballero, H. Bhadeshia, K.J.A. Mawella, D.G. Jones, P. Brown, Design of novel high strength bainitic steels: Part 1, *Mater. Sci. Technol.* 17 (2001) 512–516.
- [20] R. Veerababu, R. Balamuralikrishnan, K. Muraleedharan, M. Srinivas, Investigation of Clusters in Medium Carbon Secondary Hardening Ultra-high-strength Steel After Hardening and Aging Treatments, *Metall. Mater. Trans. A.* 46 (2015) 2455–2468. doi:10.1007/s11661-015-2843-2.
- [21] R. Veerababu, R. Balamuralikrishnan, K. Muraleedharan, M. Srinivas, Three-Dimensional Atom Probe Investigation of Microstructural Evolution during Tempering of an Ultra-High-Strength High-Toughness Steel, *Metall. Mater. Trans. A.* 39 (2008) 1486–1495. doi:10.1007/s11661-007-9333-0.
- [22] B. Sundman, B. Jansson, J.-O. Andersson, The Thermo-Calc databank system, *Calphad.* 9 (1985) 153–190. doi:10.1016/0364-5916(85)90021-5.
- [23] L.E. Iorio, The Effect of Increasing Carbon Level on Titanium Carbosulfides and Their Influence on Toughness in Ultra-high Strength Steels, PhD Thesis, Carnegie Mellon University, Pittsburgh, USA 2000.

- [24] V. Leskovšek, B. Šuštaršič, G. Jutriša, The influence of austenitizing and tempering temperature on the hardness and fracture toughness of hot-worked H11 tool steel, *J. Mater. Process. Technol.* 178 (2006) 328–334. doi:10.1016/j.jmatprotec.2006.04.016.
- [25] F. Pan, P. Ding, S. Zhou, M. Kang, D.V. Edmonds, Effects of silicon additions on the mechanical properties and microstructure of high speed steels, *Acta Mater.* 45 (1997) 4703–4712. doi:10.1016/S1359-6454(97)00121-3.
- [26] X. Zhou, F. Fang, G. Li, J. Jiang, Morphology and Properties of M_2C Eutectic Carbides in AISI M2 Steel, *ISIJ Int.* 50 (2010) 1151–1157.
- [27] G.R. Speich, D.S. Dabkowski, L.F. Porter, Strength and toughness of Fe-10Ni alloys containing C, Cr, Mo, and Co, *Metall. Trans.* 4 (1973) 303–315. doi:10.1007/BF02649630.
- [28] R. Ayer, P.M. Machmeier, Microstructural basis for the effect of chromium on the strength and toughness of AF1410-based high performance steels, *Metall. Mater. Trans. A.* 27 (1996) 2510–2517. doi:10.1007/BF02652345.
- [29] M.L. Schmidt, M.J. Gore, Solution Treatment Effects in AF 1410 Steel, in: *Proc. 34th Sagamore Army Mater. Res. Conf. Titled Innov. Ultrah.-Strength Steel Technol.*, Lake George, New York, 1987: p. 407.
- [30] E.-S. Lee, W.-J. Park, J.Y. Jung, S. Ahn, Solidification microstructure and M_2C carbide decomposition in a spray-formed high-speed steel, *Metall. Mater. Trans. A.* 29 (1998) 1395–1404. doi:10.1007/s11661-998-0354-0.
- [31] M.R. Ghomashchi, Quantitative microstructural analysis of M2 grade high speed steel during high temperature treatment, *Acta Mater.* 46 (1998) 5207–5220. doi:10.1016/S1359-6454(98)00110-4.
- [32] K.C. Hwang, S. Lee, H.C. Lee, Effects of alloying elements on microstructure and fracture properties of cast high speed steel rolls: Part I: Microstructural analysis, *Mater. Sci. Eng. A.* 254 (1998) 282–295. doi:10.1016/S0921-5093(98)00626-1.
- [33] L. Chen, J. Pei, F. Li, Y. Zhang, M. Wang, X. Ma, Decomposition Reaction of Metastable M_2C Carbide in a Multi-Component Semi-High-Speed Steel, *Metall. Mater. Trans. A.* 47 (2016) 5662–5669. doi:10.1007/s11661-016-3795-x.
- [34] R. Ayer, P.M. Machmeier, Transmission electron microscopy examination of hardening and toughening phenomena in Aermet 100, *Metall. Trans. A.* 24 (1993) 1943–1955. doi:10.1007/BF02666329.
- [35] R. Veerababu, R. Balamuralikrishnan, K. Muraleedharan, M. Srinivas, Defence Metallurgical Research Laboratory, Hyderabad DMRL TR 443, 2008.
- [36] ImageJ, Softonic. (n.d.). <http://imagej.en.softonic.com/> (accessed December 28, 2013).
- [37] E. Chang, C.Y. Chang, C.D. Liu, The effects of double austenitization on the mechanical properties of a 0.34C containing low-alloy Ni-Cr-Mo-V steel, *Metall. Mater. Trans. A.* 25 (1994) 545–555. doi:10.1007/BF02651596.
- [38] S. Lee, L. Majno, R.J. Asaro, Correlation of microstructure and fracture toughness in two 4340 steels, *Metall. Trans. A.* 16 (1985) 1633–1648. doi:10.1007/BF02663019.
- [39] S.C. Lee, F.J. Worzala, Fracture Behavior of AISI M-2 High Speed Tool Steel, *Metall. Trans. A.* 12 (1981) 1477–1484. doi:10.1007/BF02643693.
- [40] A. Shokuhfar, Z. Wallphy, The effects of heat treatment variables on the microstructure and properties of ultra-high strength steels differing in titanium content, *J. Mater. Sci.* 31 (1996) 2051–2057. doi:10.1007/BF00356626.
- [41] D. Webster, Development of a high strength stainless steel with improved toughness and ductility, *Metall. Mater. Trans. B.* 2 (1971) 2097–2104. doi:10.1007/BF02917537.
- [42] D.W. Hetzner, W. Van Geertruyden, Crystallography and metallography of carbides in high alloy steels, *Mater. Charact.* 59 (2008) 825–841. doi:10.1016/j.matchar.2007.07.005.

- [43] G.Y. Lai, W.E. Wood, R.A. Clark, V.F. Zackay, E.R. Parker, The effect of austenitizing temperature on the microstructure and mechanical properties of As-quenched 4340 steel, *Metall. Trans.* 5 (1974) 1663–1670.
- [44] R. Veerababu, Microstructural studies on high Cr-Mo secondary hardening ultra-high strength steels, PhD Thesis, Indian Institute of Science, Bangalore, India 2015.
- [45] H.K. Moon, K.B. Lee, H. Kwon, Influences of Co addition and austenitizing temperature on secondary hardening and impact fracture behavior in P/M high speed steels of W–Mo–Cr–V(–Co) system, *Mater. Sci. Eng. A.* 474 (2008) 328–334. doi:10.1016/j.msea.2007.04.014.
- [46] C. Kim, V. Biss, W.F. Hosford, A New Procedure for Determining Volume Fraction of Primary Carbides in High-Speed and Related Tool Steels, *Metall. Trans. A.* 13 (1982) 185–191. doi:10.1007/BF02643307.
- [47] D.P. Koistinen, R.E. Marburger, A general equation prescribing the extent of the austenite-martensite transformation in pure iron-carbon alloys and plain carbon steels, *Acta Metall.* 7 (1959) 59–60. doi:10.1016/0001-6160(59)90170-1.
- [48] B.M. Wilson, W.N. Weins, Retained Austenite and Tooling Failure Case Studies, in: 20th ASM Heat Treat. Soc. Conf. Proc., St. Louis, MO, 2000: pp. 566–573.
- [49] M. Naderi, A. Saeed-Akbari, W. Bleck, The effects of non-isothermal deformation on martensitic transformation in 22MnB5 steel, *Mater. Sci. Eng. A.* 487 (2008) 445–455.
- [50] M. Nikraves, M. Naderi, G.H. Akbari, Influence of hot plastic deformation and cooling rate on martensite and bainite start temperatures in 22MnB5 steel, *Mater. Sci. Eng. A.* 540 (2012) 24–29.
- [51] M. Eriksson, M. Oldenburg, M.C. Somani, L.P. Karjalainen, Testing and evaluation of material data for analysis of forming and hardening of boron steel components, *Model. Simul. Mater. Sci. Eng.* 10 (2002) 277. doi:10.1088/0965-0393/10/3/303.
- [52] C.Y. Grujicic, J.J. Rayment, An examination of the validity of existing empirical formulae for the calculation of M_s temperature, *Metall. Mater. Trans. A.* 13 (1982) 328–331.
- [53] T.J. Nichol, G. Judd, G.S. Ansell, The relationship between austenite strength and the transformation to martensite in Fe-10 pct Ni-0.6 pct C alloys, *Metall. Trans. A.* 8 (1977) 1877–1883. doi:10.1007/BF02646560.
- [54] J. Wang, S. Van Der Zwaag, Stabilization mechanisms of retained austenite in transformation-induced plasticity steel, *Metall. Mater. Trans. A.* 32 (2001) 1527–1539.
- [55] C.A. Suski, de C.A.S. Oliveira, Effects of Austenitization Temperature on the Microstructure of 15BCr30 and PL22 Boron Steels, *Mater. Res.* 16 (2013) 803–810. doi:10.1590/S1516-14392013005000054.
- [56] G. Fu, D. Jin, M. Zhu, Effect of austenitizing temperature on the microstructure and mechanical properties of Nb–Ti microalloyed steel, *J. Eng. Sci. Technol. Rev.* 8 (2015) 43–50.
- [57] J. Bakajová, M. Dománková, R. Čička, S. Eglsäer, J. Janovec, Influence of annealing conditions on microstructure and phase occurrence in high-alloy CrMnN steels, *Mater. Charact.* 61 (2010) 969–974. doi:10.1016/j.matchar.2010.06.012.
- [58] M. Grujicic, Thermodynamics aided design of high Co-Ni secondary hardening steels, *Calphad.* 14 (1990) 49–59. doi:10.1016/0364-5916(90)90039-3.
- [59] D.V. Shtansky, K. Nakai, Y. Ohmori, Decomposition of martensite by discontinuous-like precipitation reaction in an Fe–17Cr–0.5C alloy, *Acta Mater.* 48 (2000) 969–983. doi:10.1016/S1359-6454(99)00364-X.
- [60] M.S. Bhat, W.M. Garrison Jr., V.F. Zackay, Relations between microstructure and mechanical properties in secondary hardening steels, *Mater. Sci. Eng.* 41 (1979) 1–15. doi:10.1016/0025-5416(79)90038-7.

- [61] N. Ridley, S. Maropoulos, J.D.H. Paul, Effects of heat treatment on microstructure and mechanical properties of Cr–Mo–3·5Ni–V steel, *Mater. Sci. Technol.* 10 (1994) 239–249. doi:10.1179/mst.1994.10.3.239.
- [62] Y. Tomita, Effect of microstructure on plane-strain fracture toughness of aisi 4340 steel, *Metall. Trans. A.* 19 (1988) 2513–2521. doi:10.1007/BF02645479.
- [63] M.E. Matarneh, The Effect of Austenitization Treatment Temperature on H-13 Tool Steel's Mechanical Properties, *Int. J. Mech. Appl.* 6 (2016) 77–82.
- [64] W.-D. Cao, X.-P. Lu, Interpretation of the Effects of High Austenitizing Temperature on Toughness Behavior in a Low Alloy, High Strength Steel, *Metall. Trans. A.* 18 (1987) 1569–1585. doi:10.1007/BF02646141.
- [65] M.F. Carlson, B.V. Narasimha Rao, The Effect of Austenitizing Temperature Upon the Microstructure and Mechanical Properties of Experimental Fe/Cr/C Steels, *Metall. Trans. A.* 10A (1979) 1273–1284.
- [66] P.J. Ennis, A. Zielinska-Lipiec, O. Wachter, A. Czyrska-Filemonowicz, Microstructural stability and creep rupture strength of the martensitic steel P92 for advanced power plant, *Acta Mater.* 45 (1997) 4901–4907. doi:10.1016/S1359-6454(97)00176-6.
- [67] K.J. Handerhan, W.M. Garrison, The effect of austenitizing temperature on the fracture initiation toughness of As- quenched hp9- 4- 20 steel, *Metall. Trans. A.* 19 (1988) 2989–3003. doi:10.1007/BF02647726.
- [68] J.M. Vitek, R.L. Klueh, Precipitation Reactions during the Heat Treatment of Ferritic Steels, *Metall. Trans. A.* 14 (1983) 1047–1055. doi:10.1007/BF02659853.